Macromolecular Research, Vol. 24, No. 12, pp 1115-1125 (2016)
DOI 10.1007/s13233-016-4147-9

www.springer.com/13233
pISSN 1598-5032 eISSN 2092-7673

Skin Penetration-Inducing Gelatin Methacryloyl Nanogels for Transdermal Macromolecule Delivery

Jeehye Kim[1], Robert Gauvin[2], Hee Jeong Yoon[1], Jin-Hoi Kim[3], Sang-Mo Kwon[4], Hyun Jin Park[5], Sang Hong Baek[6], Jae Min Cha[7,8], and Hojae Bae*[,1]

[1]College of Animal Bioscience and Technology, Department of Bioindustrial Technologies, Konkuk University, Hwayang-dong, Kwangjin-gu, Seoul 05029, Korea
[2]Quebec Center for Functional Materials (CQMF) and Department of Surgery, Faculty of Medicine, Université Laval, Quebec, Canada
[3]College of Animal Bioscience and Technology, Department of Stem Cell and Regenerative Biology, Konkuk University, Hwayang-dong, Kwangjin-gu, Seoul 05029, Korea
[4]Laboratory of Vascular Medicine & Stem Cell Biology, Department of Physiology, Pusan National University School of Medicine, Yangsan, Gyeongnam 50612, Korea
[5]School of Life Sciences and Biotechnology, Korea University, 5-ka, Anam-Dong, Sungbuk-Ku, Seoul 02841, Korea
[6]Laboratory of Cardiovascular Regeneration, Division of Cardiology, Seoul St. Mary's Hospital, The Catholic University of Korea School of Medicine, Seoul 02841, Korea
[7]Medical Device Research Center, Research Institute for Future Medicine, Samsung Medical Center, Seoul 06351, Korea
[8]Samsung Biomedical Research Institute, Samsung Advanced Institute of Technology, Samsung Electronics Co., Ltd., Seoul 06620, Korea

Received September 5, 2016; Revised September 24, 2016; Accepted September 24, 2016

Abstract: In this study, the suitability of gelatin methacryloyl (GelMA) nanogels for transdermal delivery of macromolecules was demonstrated. The synthesis of GelMA nanogels (GNs) and fluorescein isothiocyanate labelled bovine serum albumin (FITC-BSA) loaded GelMA nanogels (FGNs) were implemented when confined in water-in-oil nanoemulsion droplets *via* the photopolymerization of the methacryloyl substituents to create crosslinked nanogels. Both GNs and FGNs existed as fine particles in aqueous condition (pH 7.4) for 7 days. No distinct aggregation of nanogel particles were observed. In the MTT assay, high percentage of cell viability indicated that GNs did not exhibit any growth inhibitory effect or significant cytotoxicity. The skin penetration study results showed that FGNs permeated across the epidermis and into the dermis of a porcine model when compared to the FITC-BSA dissolved in PBS. Possible penetration routes of FITC-BSA through the stratum corneum (SC) were illustrated by visualizing the SC structure with fluorescent signals of FITC-BSA. The penetration mechanism of FGNs across the SC layer was successfully demonstrated by explaining three penetration routes (intercellular, follicular, and transcellular route). The results suggest that GNs have a potential as a transdermal delivery carrier for hydrophilic macromolecules.

Keywords: nanogels, transdermal delivery, intracellular protein delivery, photocrosslinkable polymers, biodegradable polymers, polymeric carrier.

Introduction

Various types of therapeutic approaches involving nanotechnologies have been widely investigated for drug delivery applications.[1,2] However, delivery of biologically active molecules using nanotechnology is still limited due to the lack of stability and short systemic circulation time of carriers *in vivo*, which result from their poor solubility, limited bioavailability, rapid elimination in biological conditions and lack of penetrability across anatomical and physiological barriers.[3-5] On the other hand, hydrogels, which can be defined as three-dimensional (3D) cross-linked networks of water-soluble polymers, have made considerable progress in drug delivery applications.[6] However, they have often showed limitation resulting from failure to control release of drugs mainly caused by their high water content and large pore size.[5,7,8] Recently, some advances have been made in nanogel technologies to provide new strategies addressing the problems associated for drug delivery application.[9]

Nanogels are a promising alternative to conventional nanotherapeutic approaches. They are composed of cross-linked 3D polymeric particles with submicrometer size.[10] In other

*Corresponding Author. E-mail: hojaebae@konkuk.ac.kr

words, the internal structure of nanogels is similar to that of hydrogels, but nanogels have homogeneous particle size diameter ranging from 10 to 200 nm.[11] As fine polymeric particles, nanogels have two distinct features which play an important role in controlling drug release. First, nanogels are very stable in biological fluids due to their negligible van der Waals reciprocal forces of attraction, thus prohibiting particles aggregation.[12] Second, nanogels containing hydrophilic functional groups, such as hydroxyl (-OH), carboxyl (-COOH), amino ($-NH_2$), amide ($-CONH_2$) and sulfonic ($-SO_3H$) groups, are used to fabricate the fine network structure of polymer chains, which allows to control the release rate of drugs from the polymer networks.[13] With those features related to their fine size and the extent of functional groups available, nanogels therefore present advantages over conventional therapeutic approaches.

One of the important characteristics of nanogels in controlling drug release is their swelling properties in aqueous environment. The extent of swelling capacity of nanogels is comparable to that of bulk state (*i.e.*, hydrogels) since they have similar internal structures. However, their rapid swelling and contraction derived from the features of nanoparticles such as high-surface area and overall sizes in the range of cellular compartments are distinctive. They can be controlled by altering the gel particle diameter in aqueous phase and the cross-linking density of the gel network.[4] The tunable swellability has a significant role in the control of the amount of drugs loaded into the gel matrix and subsequent drug release through the gel network.[7]

Another important property of nanogels as a delivery agent is their biodegradability. While non-biodegradable polymers could potentially be accumulated in tissues and cause irritation, they are generally non-reactive in the human body and can be metabolized and evacuated *via* normal metabolic pathways.[14] Biodegradation of the polymers composed of nanogels involves cleavage of hydrolytically or enzymatically sensitive bonds, which results in scission of the polymer chains.[15] Therefore, the extent of drug release from nanogel matrices can be controlled by varying the physical properties of the gels such as swelling and biodegradation.

Transdermal drug delivery (TDD) has many advantages over oral delivery since it has been proven beneficial to reduce dose frequency by offering sustainable drug release from delivery carriers, thus avoiding hepatic first pass metabolism and degradation in the gastrointestinal tract and therefore achieving target specific delivery.[16,17] Numerous delivery approaches involving nanotechnologies have been highlighted to effectively transport biological macromolecules (*e.g.*, proteins, peptides, or genes) but the transdermal delivery of macromolecules is still at an early stage in development. To this end, nanogels have been developed by combining the advantages of hydrogels such as biocompatibility, biodegradability and high water content with the characteristics of nanoparticles like high surface area and fine particle size, offering the opportunity for improved skin penetration efficacy of biologically active molecules. To accomplish the TDD, drug-encapsulated carriers should successfully pass through the skin by reversibly disrupting the stratum corneum (SC), the outmost layer of skin, to reach the targeted site (*e.g.*, fibroblasts in dermis for treatment of keloids, skin accumulation in epidermis of ultraviolet (UV) absorbers for UV protection).[17,18] Specifically, the greatest challenge of TDD comes from the high lipophilicity of the SC layer and consequently, only a limited number of hydrophobic drugs with small molecular masses that are up to few hundred Daltons are suitable for passing through the SC.[19] Hypodermic injection could be an option to overcome the limitation associated with crossing the hydrophobic layer, but many formulations containing drugs are not adequately deformable to be injected, requiring surgical implantation to obtain suitable results.[7] Other approaches such as chemical enhancers, iontophoresis, ultrasound and electroporation were successful in enhancing skin permeability, but those are still limited for transdermal delivery therapies due to skin irritation and/or potential toxicity to cells found in the various skin layers.[16] In this context, nanogels are promising to address the limitations regarding the delivery of hydrophilic macromolecules and skin irritation problems in TDD systems. Nanogels is an applicable vehicle system to transport hydrophilic molecules such as proteins and peptides into the skin since their small size is appropriate to penetrate the tissue and they are composed of polymer chains well adapted for encapsulation of hydrophilic bioactive molecules. In addition, nanogels swell and subsequently dissolve in an aqueous environment, thus possible to engineer formulations tailoring their mechanical properties by varying the molecular weights and adjusting the cross-linking density for diverse topical application intended for specific clinical uses.[20] Nanogels also show good biocompatibility and biodegradable properties, which reduces concerns about irreversibly disrupting skin structures and cytotoxicity.[10,14]

Therapeutic applications of nanogel technology have been studied in the past few decades, mainly investigated for oral delivery and hypodermic injection.[21,22] However, successful delivery of biologically active molecules through transdermal route has been rarely explored.[23] Herein, our work highlighted great potential of nanogel technology for transporting hydrophilic macromolecules across the SC.

Experimental

Materials. Gelatin from porcine skin (Type A, 300 bloom), methacrylic anhydride (MA), *N*,*N*-dimethylformamide (DMF), n-octane, albumin-fluorescein isothiocyanate conjugate were purchased from Sigma-Aldrich (St. Louis, MO, USA). Sorbitan monooleate (Span 80) and polyethylene glycol sorbitan monooleate (Tween 80) were purchased from Samchun Pure Chemical (Pyeongtaek, South Korea). Photoinitiator, Irgacure 2959, was purchased from BASF (Minden, Germany). The porcine skins for penetration study were purchased

from Medikinetics (Pyeongtaek, South Korea).

Synthesis of Gelatin Methacryloyl (GelMA). The synthesis of gelatin modified with methacrylic anhydride was reported by Nichol *et al.*[24] Briefly, type A porcine skin gelatin was added into 10% (w/v) Dulbecco's phosphate buffered saline (DPBS, Gibco, USA) at 60 °C and stirred until fully dissolved. MA was added at a rate of 0.5 mL/min to the gelatin solution and stirred at 50 °C for 1 h. The fraction of lysine groups reacted with MA existing in the reaction mixture. After the dilution with additional warm (40 °C) DPBS (5 times) to stop the reaction, the resulting mixture was dialyzed against distilled water using 12-14 kDa cut-off dialysis tubing for a week at 40 °C to remove salts and unreacted monomers. The solution was lyophilized and stored at 4 °C until further use.

Fabrication of GelMA Nanogels (GNs). GNs were prepared using water-in-oil (W/O) emulsions referred to inverse emulsions as a template. Briefly, GelMA was mixed into PBS (pH 7.4) containing 0.5% (w/w) photo-initiator (PI) (Irgacure 2959, BASF) and stirred at 60 °C until fully dissolved. The resulting clear dispersion was added to *n*-octane containing Span 80 and Tween 80 surfactant mixtures. The resulting mixture was high-speed homogenized for 5 min to get crude emulsions, and further homogenized using ultrasonic processor (VC 505, Sonic & Materials, USA) under 20 watts to get fine and homogeneous emulsions. The samples were kept at 4 °C during the whole process. The resulting fine emulsions were placed overnight at room temperature to reach equilibrium. The stability of the resulting inverse nanoemulsions was observed and if qualified as stable (*i.e.*, homogeneously transparent without sedimentation), the region was marked in a ternary phase diagram (Figure 1). According to the result from the study, a certain proportion of aqueous phase/surfactants/organic phase (16.7:16.7:66.7) was selected for further experiments. The emulsions were exposed to UV light for 30 min under irradiance level of 10 W/cm^2 using a 250-450 nm light source, under mild stirring, at a distance of 30 mm from the UV lamp. After polymerization, the cross-linked nanogels were recovered by the addition of tetrahydrofuran (THF). The mixtures were centrifuged for 10 min (8,000 g) to remove organic phase and surfactants. After removing the supernatant, THF was added and the same procedure was repeated 2 times. The precipitates were then dried and redispersed in 5 mL of PBS (pH 7.4) and stored at the room temperature before further use.

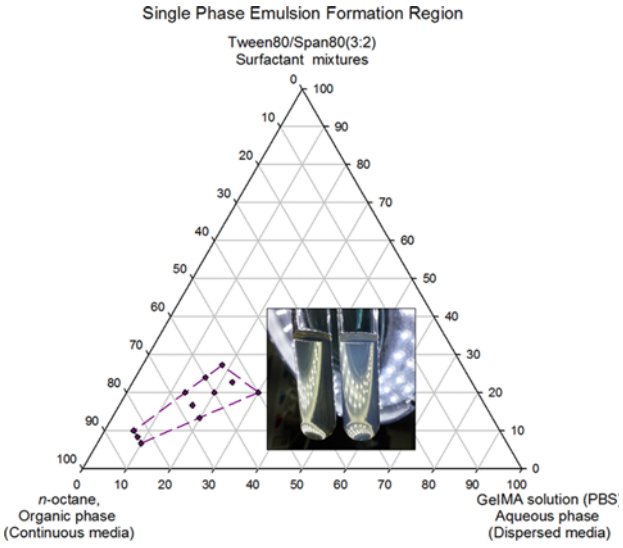

Figure 1. Ternary phase diagram for water-in-oil nanoemulsions composed of n-octane, surfactant mixtures and aqueous phase. Marked quadrangle area depicts the conditions in which fine and homogeneous water-in-oil nanoemulsions can be formed. The image in the ternary diagram indicates that the water-in-oil nanoemulsions are transparent and no phase separation is occurring.

FITC-BSA Loaded GelMA Nanogels. FITC-BSA was loaded in the nanogels during nanogels preparation. Briefly, FITC-BSA was added to GelMA dispersion including 0.5% PI to obtain final concentration of 0.2% (w/w) in each hydrogel. FITC-BSA (0.2% w/w) dissolved in PBS was prepared as a control group. The resulting solutions were mixed with the organic phase containing surfactant mixtures and further homogenized by high-speed homogenizer and ultrasonic processor. The stable dispersion was exposed to the UV light for 30 min under irradiance level of 10 W/cm^2. The FITC-BSA loaded nanogels (FGNs) and the control sample were isolated through precipitation with THF, dispersed in 5 mL of PBS (pH 7.4) and stored at the room temperature before further use.

Size and PDI Measurements. Hydrodynamic diameter and PDI of nanogels were measured during and after nanoagels preparation by dynamic light scattering (DLS) using a nano size analyzer (Malvern Zetasizer Nano ZS, Malvern Instruments, UK). The hydrodynamic diameters were calculated from diffusion coefficients using the Strokes-Einstein equation. Samples (n=3) were diluted for measurement, and each measurement was performed in triplicate.

Morphology of GNs. The morphology of FGNs was visualized using a transmission electron microscope (TEM) (TECNAI G2 F30, Philips-FEI, Holland). To perform TEM observation, nanogels were dropped onto formvar·carbon coated grid and dried for 30 s and the excess was drawn off with membrane filter paper. This step was performed two times. The grid was stained with Platinum blue to enhance the contrast and then dried overnight at room temperature.

Cytotoxicity Assay. Cell viability was evaluated using a MTT cell proliferation assay kit (Duchefa biochemie, Holland). The murine fibroblast NIH3T3 cells (1×10^4 cells/well) were seeded onto 96-well plates and cultured in Dulbecco's modified Eagle's medium (DMEM, WELGENE, Korea) supplemented with 10% bovine calf serum (BCS, WELGENE, Korea) in a humidified atmosphere (5% CO_2/95% O_2/37 °C). The dried GNs were dispersed at serial concentrations of 0.5, 1, 2, and 5 mg/mL, respectively. For each concentration, 100 μL of GNs was deposited in each well to replace the culture medium. Each sample was tested in eight replicates per plate.

After incubation, 100 μL of culture medium containing the MTT solution was replaced with the nanogels dispersion in each well. The plates were then incubated for 3 h. Then, the supernatant solution was removed. DMSO of 100 μL was added to each well to dissolve the formazan crystals. The optical density was measured using a microplate reader at 550 nm. Cell viability was determined as a percentage of control (untreated cell).

Skin Penetration Study. The skin penetration studies were performed using a Franz Diffusion Cell (PermeGear, USA) with an effective diffusion area of 2.27 cm^2 and a receptor volume of 15.9 mL. The porcine skin samples of 700 μm thickness using a dermatome were obtained from Micropig (Medikinetics, South Korea). The porcine skin was thawed at room temperature and rehydrated in PBS (pH 7.4) for 1 h before the experiment. The skin sample was placed between the donor and receiver compartments, which was then securely fastened with a clip. The receiver compartment was filled with PBS (pH 7.4) and continuously stirred at 600 rpm at 37 °C for 1 h to equilibrate the skin. After equilibration, 1 mL of the 0.2% FGNs and 0.2% w/w FITC-BSA dispersed in PBS (pH 7.4) (control) were dropped slowly on the donor compartment to cover the nanogels on the skin surface. The skin permeation studies were performed at predetermined times.

Microscope Observation. After the skin permeation experiment, the residual FGNs on the skin surface were gently removed with pipetting. The skin samples were sectioned (>10 sections from each sample) vertically to a thickness of 30 μm. Immediately after, the skin sample was taken from the diffusion cell and placed on a slide glass for further microscope observation. To demonstrate permeation of FGNs into the dermis, a cryostat-microtome (CM3050S, LEICA, Wetzlar, Germany) was used to vertically section the skin sample. Permeation profiles were obtained using CLSM (LSM 700, Carl Zeiss, Jena, Germany). To investigate penetration routes of FITC-BSA and SC structure, the images of cross and vertical sections of porcine skin were taken using CLSM optical sectioning.

Statistical Analysis. Nanogel diameters and MTT cell proliferation assay data were analyzed using one-way ANOVA by concentrations of GNs and FGNs as well as culture time as independent variables. *Post hoc* analysis was performed with Fisher's LSD test. All analysis was performed using GB-STAT v8.0 (Dynamic microsystems, USA). A p-value < 0.05 was considered to indicate statistical significance.

Results and Discussion

Synthesis of GNs. The synthesis of gelatin modified with MA was done by introducing methacryloyl substitution groups to the reactive amine and hydroxyl groups of the amino acid residues to make gelatin methacryloyl (GelMA).[25] Specifically, the addition of methacryloyl substituent groups enebled to covalently crosslink the gel network through a photopolymerization under UV light in the presence of a photoinitiator (PI).[26] After the synthesis of GelMA, a ternary phase diagram study was implemented to determine the appropriate mixture ratio of GelMA (dissolved in PBS solution), *n*-octane and surfactants to form stable water-in-oil nanoemulsions (Figure 1). In Figure 1, the marked quadrangle area indicates that there are a limited set of conditions in which fine and homogeneous nanoemulsions could be formed without sedimentation. To form stable water-in-oil nanoemulsions, a mixture of Span 80 and Tween 80 surfactants was selected followed by high-speed homogenization. Since it is known that water-in-oil emulsions are relatively less stable than oil-in-water emulsions, due to the increased attraction between particles resulting from the polarity of the organic phase dispersion medium.[27] The results from Figure 1 and Supplementary Figure S1 indicate that fine and homogeneous nanoemulsions were formed only under certain weight ratios of water/oil/surfactant mixtures. Therefore, the weight ratio of water/oil/surfactant (1:4:1) was selected for further preparation of GNs. Schematic representation illustrating the preparation of GNs is shown in Figure 2. Briefly, 5% GelMA aqueous solution containing 0.5% w/w photoinitiator (PI) was homogenized with the organic phase and the surfactants in the predetermined mixture ratio of water/oil/surfactant to fabricate GNs confined in nanoemulsion droplets (Figure 2(A) and 2(B)). Photocrosslinking of the GNs were conducted under UV light to create a covalently crosslinked gel network of the methacryloyl substituents grafted on the gelatin (Figure 2(B) and 2(C)). The resulting solution containing GNs was then purified to completely eliminate the surfactants and organic phase, which are cytotoxic if not removed and the purified GNs were dispersed in PBS (pH7.4) (Figure 2(C) and 2(D)).

Characterization of GNs. During and after the preparation of GNs, hydrodynamic diameter and polydispersity index (PDI) of GelMA nanogel particles were calculated using Dynamic Laser Scattering (DLS), which measures the diffusion of small particles moving under Brownian motion and allows to calculate the hydrodynamic diameter using the Strokes-Einstein relationship. This technique was used at each preparation step of GNs to investigate the effect of photopolymerization on the size evolution and swelling properties of GN particles, as well as to record size change during the storage at room temperature. As illustrated in Figure 3(A), the size distribution of GNs and FGNs was narrow when dispersed in PBS immediately after the nanogels preparation. This demonstrates that the nanogels display homogeneous particle size and remain as fine particles in aqueous condition. In Figure 3(B), the morphology of the FGNs in dried state was visualized using a TEM. The TEM image showed clusters of fine polymeric particles of spherical shape. The comparable size between the FGN particles shown in Figure 3(B) corresponded well with the low PDI results obtained from the DLS in Figure 3(A). Therefore, this shows that GNs existed with a controllable size range distribution in a dried state as well as

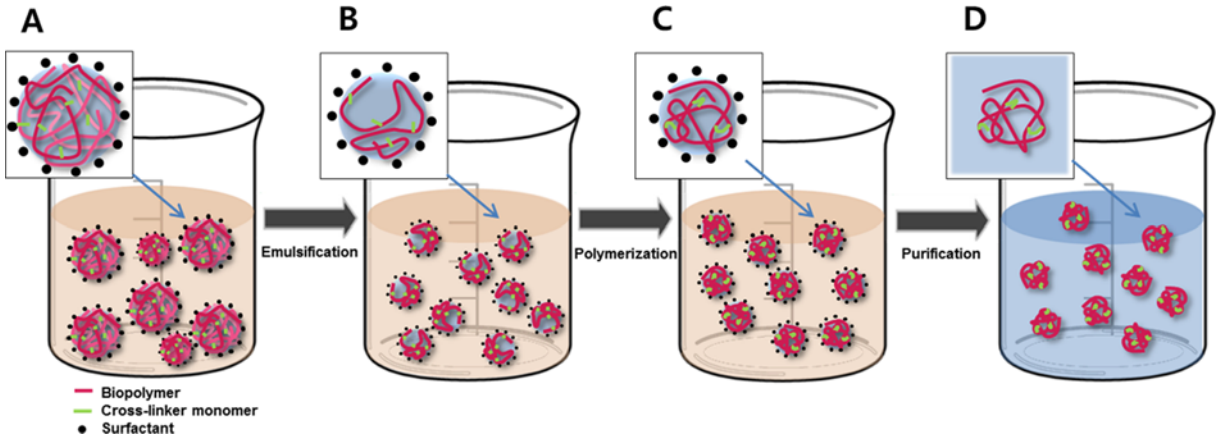

Figure 2. Schematic representation of the procedures to prepare GNs. The aqueous solutions containing the GelMA and the PI were mixed and homogenized with the organic phase and surfactants to form stable and fine polymeric nanoparticles confined in water-in-oil nanoemulsions; (A and B). The methacryloyl substituent groups of polymeric nanoparticles were photocrosslinked under UV light to create fine gel networks; (B and C). The resulting nanogel particles were purified to remove remaining surfactants and organic phase and were dispersed in PBS (pH 7.4); (C and D).

in swollen state, indicating that the synthesized polymeric particles are stable through the changes in aqueous/dried conditions. Additional TEM images were presented in Supplementary Figure S2, showing uniform spherical shape and diameters ranging approximately from 150 nm up to 250 nm in dried state. In Figure 3(C), the changes in hydrodynamic diameter indicated that GNs were swollen in physiological fluid while they did not show the same swelling properties when confined in nanoemulsions (both before and after UV polymerization). Figure 3(C) also shows that the UV exposure for polymerization did not affect the size evolution of GNs. Rather than showing increased particle size, GNs slightly shrank, which suggested that the GelMA confined in droplets was crosslinked and created a compact gel network after photopolymerization. According to the statistical analysis from Fischer's Least Significant Difference (Fischer's LSD), hydrodynamic diameters of nanogels significantly decreased ($P < 0.05$) after UV polymerization in both GNs and FGNs. However, hydrodynamic diameters of nanogels significantly increased ($P < 0.05$) when nanogels were redispersed in PBS, representing swelling of GNs in aqueous condition. Interestingly, the hydrodynamic diameters of GNs dispersed in PBS were significantly greater than those of FGNs dispersed in PBS ($P < 0.05$). Since FITC-BSA carries negative charge under pH 7.4 condition, the formation of intermolecular linkages (electrostatic force) with positively charged amino groups of gelatin may be assumed to influence the hydrodynamic diameter difference.[25,28]

GNs and FGNs showed high degree of dispersion stability in PBS solution as depicted in Figure 3(D). The changes in hydrodynamic diameter and PDI of the GNs were recorded for 7 days. The blue lines representing hydrodynamic diameters show that there was no aggregation between the particles. The red lines, indicating the PDI, demonstrated that the GN particles and FGN particles in PBS dispersion were homogeneous during the storage. In other words, both GNs and FGNs were stable in physiological-like fluid (pH 7.4, PBS solution). To create GNs presenting a high degree of suspension stability, repulsive forces between nanoparticles must exist to overcome the van der Waals forces. As shown in Figure 3(D), both GNs and FGNs showed good suspension stability up to one week.

Influence of GelMA Nanogels on Cell Viability. It has been reported that GelMA-based hydrogels are biocompatible, biodegradable, non-cytotoxic, and nonimmunogenic.[25] However, the low-molecular-weight residues including unreacted MA and methacrylic acid byproducts are potentially cytotoxic if not removed completely after the synthesis. Also, the PI residues, organic phase and surfactants remaining after the synthesis of GNs may cause negative consequences on the cells and tissues. To elucidate the biocompatibility of the GNs in a physiological environment and at the cellular level, the cytotoxic effect of GNs was evaluated with increasing concentrations (0.5, 1, 2, and 5 mg/mL) and analyzed using the MTT cell proliferation assay. In Figure 4, the cytotoxicity profile of GNs after 24 and 72 h demonstrated that the nanogels did not affect cell proliferation and showed that cells incubated with GNs remained viable up to 5 mg/mL.

Penetration Profiles of FGNs. FGNs were prepared to detect the permeation of BSA through the skin structure and therefore to visualize the passage of the molecule. BSA was used as a model drug due to the well-defined molecular weight (66.5 kDa) to demonstrate that the GNs represent a suitable system to deliver hydrophilic macromolecules such as peptides and proteins across the SC. Porcine skin samples were prepared to perform permeation study using a Franz diffusion cell. The skin samples with 700 μm thickness were measured and sectioned using a dermatome to be used for microscope

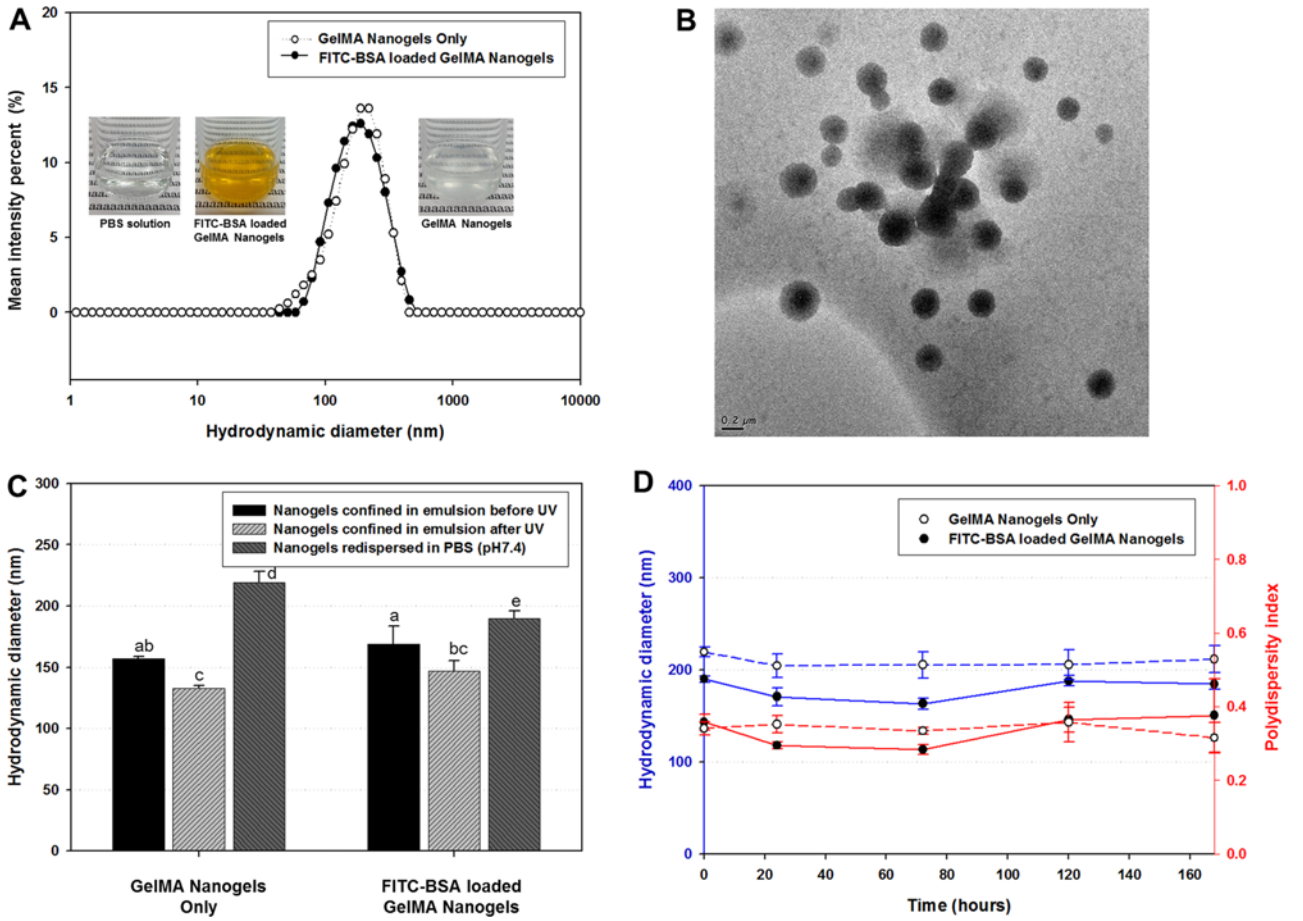

Figure 3. Characterization of GNs and FGNs. Both GNs and FGNs showed narrow size distribution dispersed in PBS immediately after GelMA nanogel preparation (left: PBS solution, center: FGNs, right: GNs) (A). TEM image of FGNs on the formvar·carbon-coated grid in dried state indicated that the nanogel particles kept their integrity (scale bar=0.2 μm) (B). Hydrodynamic diameters of GNs confined in emulsion (before and after UV polymerization) and GNs dispersed in PBS showing that GNs were swollen in the aqueous phase. Letters indicate a significant difference at $P<0.05$ (Fischer's LSD) (C). GNs and FGNs showed stable evolution kinetics of both hydrodynamic diameter and PDI in PBS and no aggregation happened over time (168 h total). Samples were stored at room temperature for a week. Data are plotted as the mean ± standard deviation (n=3) (D).

observation, as whole porcine skin (> 2 mm) was found to be too thick to be optically sectioned by Confocal Laser Scanning Microscope (CLSM). Therefore, the resulting skin sample was composed of the SC, a viable epidermis and a portion of the dermis. Skin permeation studies were performed at predetermined times (12 and 24 h). The residual FGNs on the skin surface were gently removed with a pipette and the drug penetration profiles were characterized.

To analyze the penetration profile, a vertical cryotome-section of the whole skin layer (SC, epidermis and a portion of the dermis) was imaged using a CLSM and a fluorescence microscope. In this study, FITC-BSA of 0.2% w/w was used as a fluorescent tag to demonstrate the permeation of the FITC-BSA into the skin membrane. Then, 1 mL FGNs of and FITC-BSA in PBS solution (control) was dropped slowly on each donor compartment of the Franz Diffusion Cells to cover the skin surfaces. One milliliter of each sample contained an equal amount of FITC-BSA (0.2% w/w). After 24 h, the remaining FGNs and control solutions were removed with a pipette to detect only the FITC-BSA absorbed in the skin layers and the skin samples were taken out immediately from the diffusion cells. Then the samples were vertically sectioned using a cryostat microtome for microscope observation. The CLSM images of vertical sections of the skin samples in Figure 5 verified that the GNs could efficiently transport the FITC-BSA into the dermis compared to the control group. As shown in Figure 5(A), (B), and (C), the green fluorescent signals illustrated that the control solution could not permeate into the deeper layer and accumulated in the SC. However, in Figure 5(D), (E), and (F), the FGNs permeated into the dermis and were accumulated in SC showing stronger fluorescent signals. Thus, the CLSM images in Figure 5 clearly demonstrated that the GNs delivered FITC-BSA into the deeper layer of the skin while the FITC-BSA dissolved in

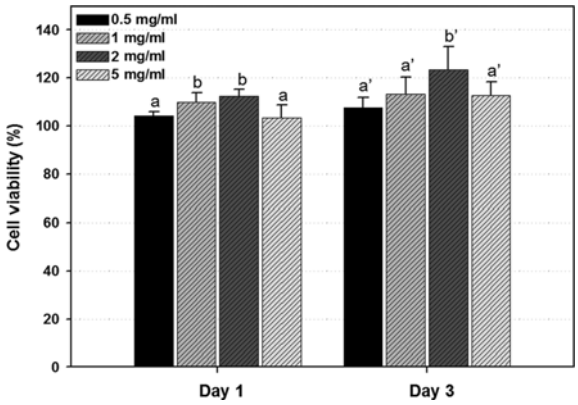

Figure 4. Influence of GNs on murine fibroblast NIH3T3 cells viability. The MTT cell proliferation assay was used to demonstrate that GN has no significant effect on cell proliferation. The experiments were repeated in triplicate for each sample (0.5, 1, 2, and 5 mg/mL). The dried nanogels were dispersed in DMEM with 10% BCS containing NIH3T3 cells at serial concentrations of 0.5, 1, 2, and 5 mg/mL and cultured for 24 and 72 h (5% CO_2 at 37 °C). Each condition was obtained in eight replicates per plate. Data are plotted as the mean ± standard deviation (n=9). Different letters indicate a significant difference on cell viability at $P < 0.05$ by the Fischer's Least Significant Difference (Fischer's LSD).

PBS could not pass through the SC.

Visualization of Stratum Corneum Structure and Drug Penetration Routes. Another approach to investigate the skin penetration profile was to visualize and analyze possible drug penetration routes by CLSM optical sectioning. It is expected that the highly impermeable nature of the SC impairs the penetration of FITC-BSA and the permeation through the SC is considered one of the major challenges in TDD. For instance, it has been reported that only 1-2% of radiolabeled hydrocortisone permeated into skin while up to 90% permeated when the SC was removed.[29] Similarly, another study found that topical anesthetics did not show any medicinal effect in the skin until they permeated into the skin in sufficient quantities after the SC removal.[30] These studies demonstrate that the SC is the main structural hurdle limiting molecule transport to the layers below the SC. As shown in Figure 5, the green fluorescent signals demonstrated that the FGNs successfully permeated into the layers below the SC (Figure 5(D) and (F)), but it is unclear how the FGNs passed through the SC structure. Therefore, the configuration of SC composed of corneocytes and intercellular multilamellar structures was mainly visualized and discussed in Figure 6 to elucidate the penetration mechanism of FGN. The results from CLSM

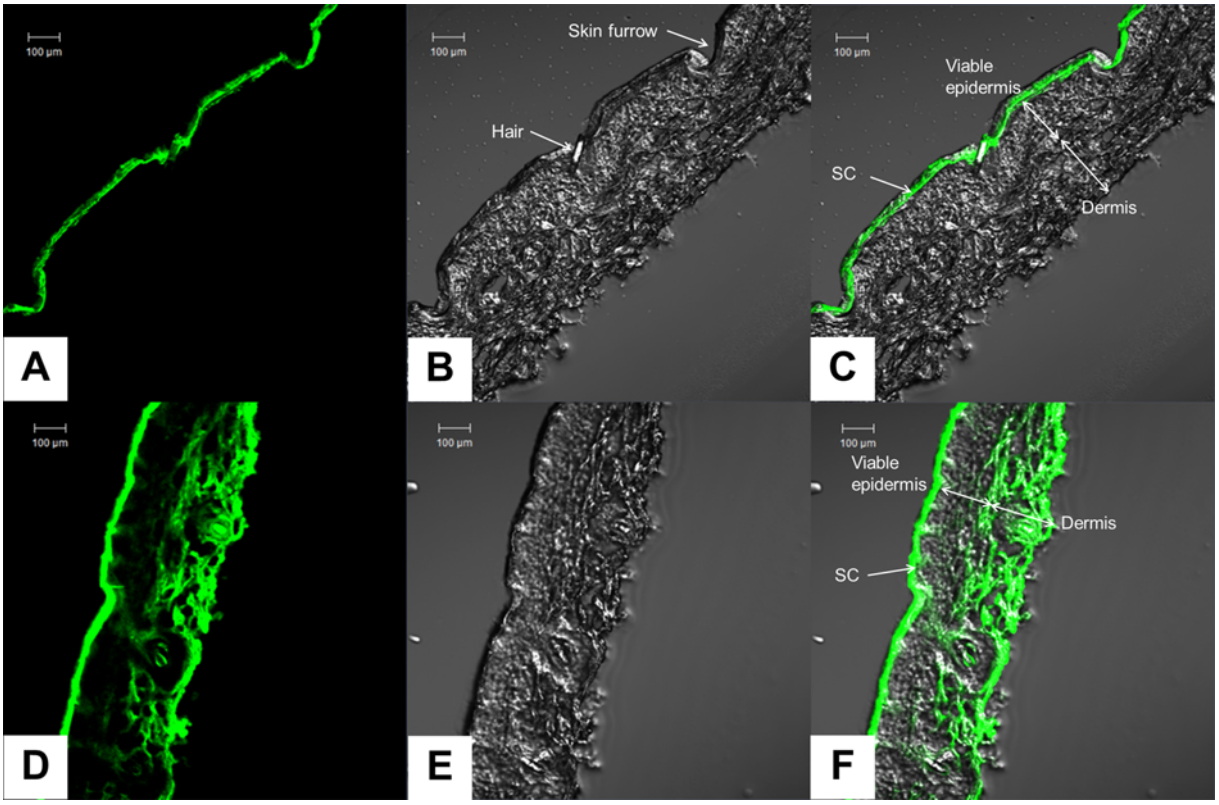

Figure 5. Confocal images of porcine skin. FITC-BSA (0.2% w/w) was used as a fluorescence tag to demonstrate the permeability of the FITC-BSA into the skin. One milliliter of the FITC-BSA (0.2% w/w) dissolved in PBS (pH7.4) and the same amount of FGNs were placed on each skin surface for 24 h. Microscope images show that the FITC-BSA in PBS did not permeate into deeper layer but accumulated in the SC (A, B and C). However, the FGNs permeated into the dermis and some molecules accumulated in the SC (D, E and F). The CLSM images were taken in fluorescence mode (488 nm) (A and D), DIC mode (B and E), and merge mode (C and F). (Images with scale bars=100 μm).

optical sectioning (Figure 6(A)) and additional illustration (Figure 6(B)) show that the SC constitutes skin ridges, pores and skin furrows (which are also visualized in Figure 5(B)) and is made up of cellular structures (*i.e.*, corneocytes) with multilamellar bilayers composed of ceramides, cholesterol and free fatty acids as described in Figure 6(C).

The internal structure was also investigated because the highly hydrophobic nature of the SC (which contains 13% water) derived from internal SC configuration, corneocytes and multilamellar lipid bilayers, involves different permeation pathways of macromolecules through the SC.[31] It has been reported that there are a number of possible pathways for the delivery of molecules through the SC.[32] Specifically, follicular route through the skin appendages (*i.e.*, hair follicles and sweat grands) is one of the interesting possible pathways for molecules transport because a number of studies have shown that nanoparticles accumulated preferentially in the follicular openings.[33] In this study, it was also demonstrated that the FGN accumulated preferentially in the hair follicles as shown in Supplementary Figure S3. Another possible pathway, transcellular (or intracellular) route occurs when the molecules pass the SC by crossing the corneocyte membrane and entering the cell as illustrated in Figure 6(C).[34] However, the transcellular diffusion is considered as a practically unimportant route for transdermal drug transport due to narrow aqueous transepidermal pathways.[35] Specifically, the corneocyte membranes are relatively hydrophobic and therefore, hydrophilic molecules have low solubility in this environment. In contrast, intercellular route occurs when the molecules pass through the intercellular spaces existing between corneocytes which are hydrophilic in character (Figure 6(C)). In our observation, Figure 7 successfully demonstrated the FGN transportation *via* follicular, intercellular as well as transcellular route. Specifically, no green fluorescent signals were detected on the skin surface (Supplementary Figure S4) indicating that the detected green fluorescent signals by CLSM shown in Figure 7 represented FGN that had been absorbed and accumulated within the SC during the skin permeation

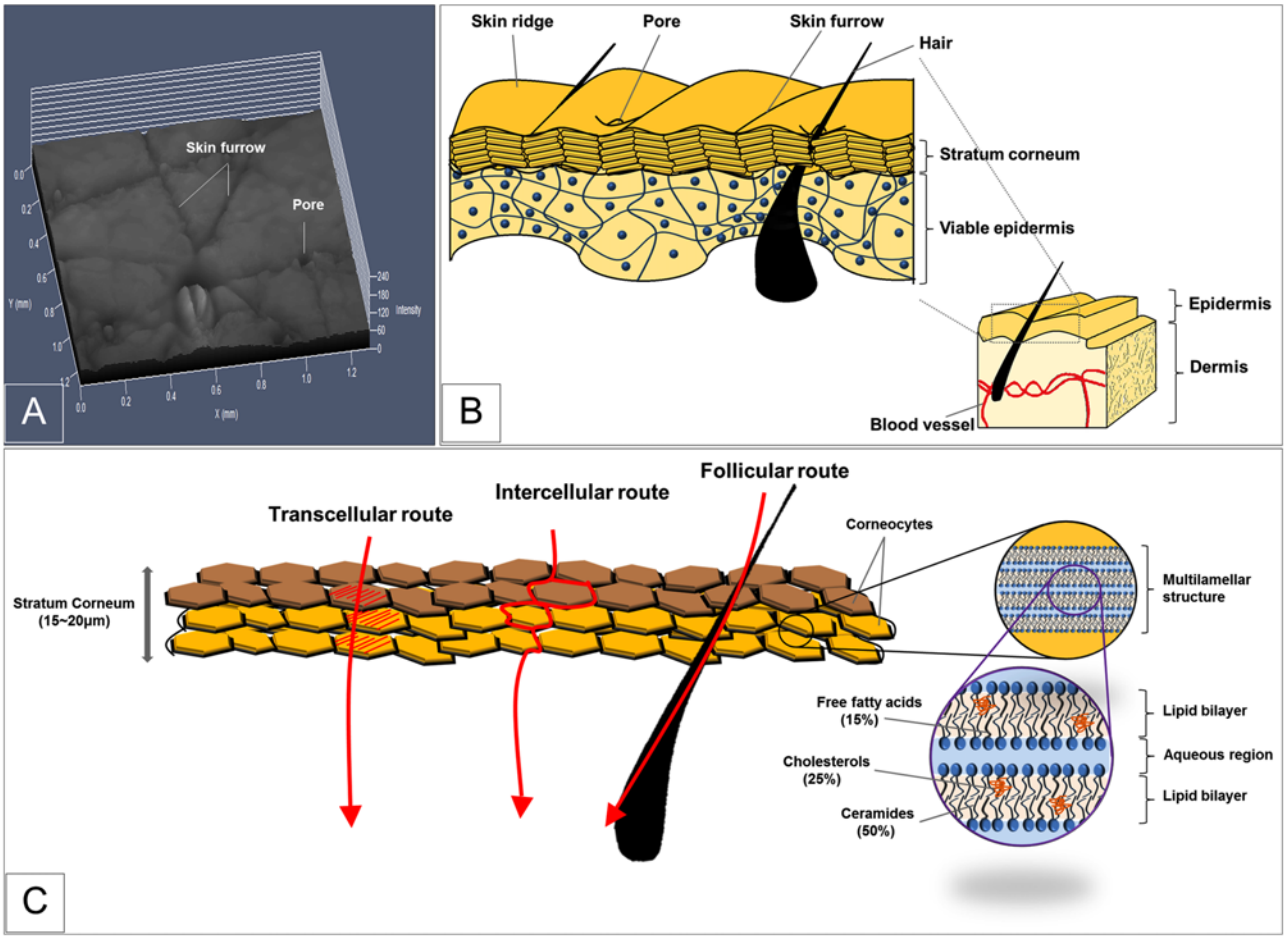

Figure 6. The CLSM optical sectioning images of the porcine skin as a series of xy-planes. The 3D structure of the SC was generated through the digitized image data of the optically sliced xy-planes (z=0-245 μm at 5 μm intervals) (A). A schematic model to describe the skin structure containing the SC, epidermis and dermis layers (B). The possible penetration routes of FGN through the SC and the internal SC structure (C).

study. The different depths of optically sectioned xy-planes were represented in Figure 7(D) to visualize the possible FGN permeation routes through the SC structure. A single image within the yellow box from Figure 7(D) was selected to elucidate the detailed permeation pathways for FGN. The optical SC structure (z=50 μm) taken in differential interference contrast (DIC) mode by CLSM is shown in Figure 7(B). The green fluorescent signals detected in fluorescence mode by CLSM are presented in Figure 7(C) to visualize FGN permeated in the SC. Then, Figure 7(B) and (C) were merged and shown in Figure 7(A). Therefore, the CLSM images of Figure 7(A), (D), and E (merge mode - DIC with fluorescence mode) optically show the SC structure with the permeation pathways of FGN represented by the green fluorescent signals. Figure 7(A) and (D) are horizontal optical sectioned images of a skin sample and Figure 7(E) is a vertical optical section of the same sample. As shown in Figure 7(A)-(C), the green fluorescent signals in the optical sections demonstrated that the transdermal diffusion of FGN through the SC occurred *via* intercellular, transcellular and follicular route. Specifically, a blue circle (left) shown in Figure 7(A) indicates that FGN is transported through the continuous lipid matrix between the corneocytes (*i.e.*, intercellular route) as net shaped green fluorescent signals can be observed.[36] The configuration and morphology of the corneocytes found in Figure 7(A) and (B) identically conformed to the flat hexagonal structure of corneocytes described in Figure 6(C) which are also reported in many references.[36-38] The strong green fluorescent signals in another blue circle (right) of Figure 7(A) indicated that FGN also transported through the hair follicle illustrated in Figure

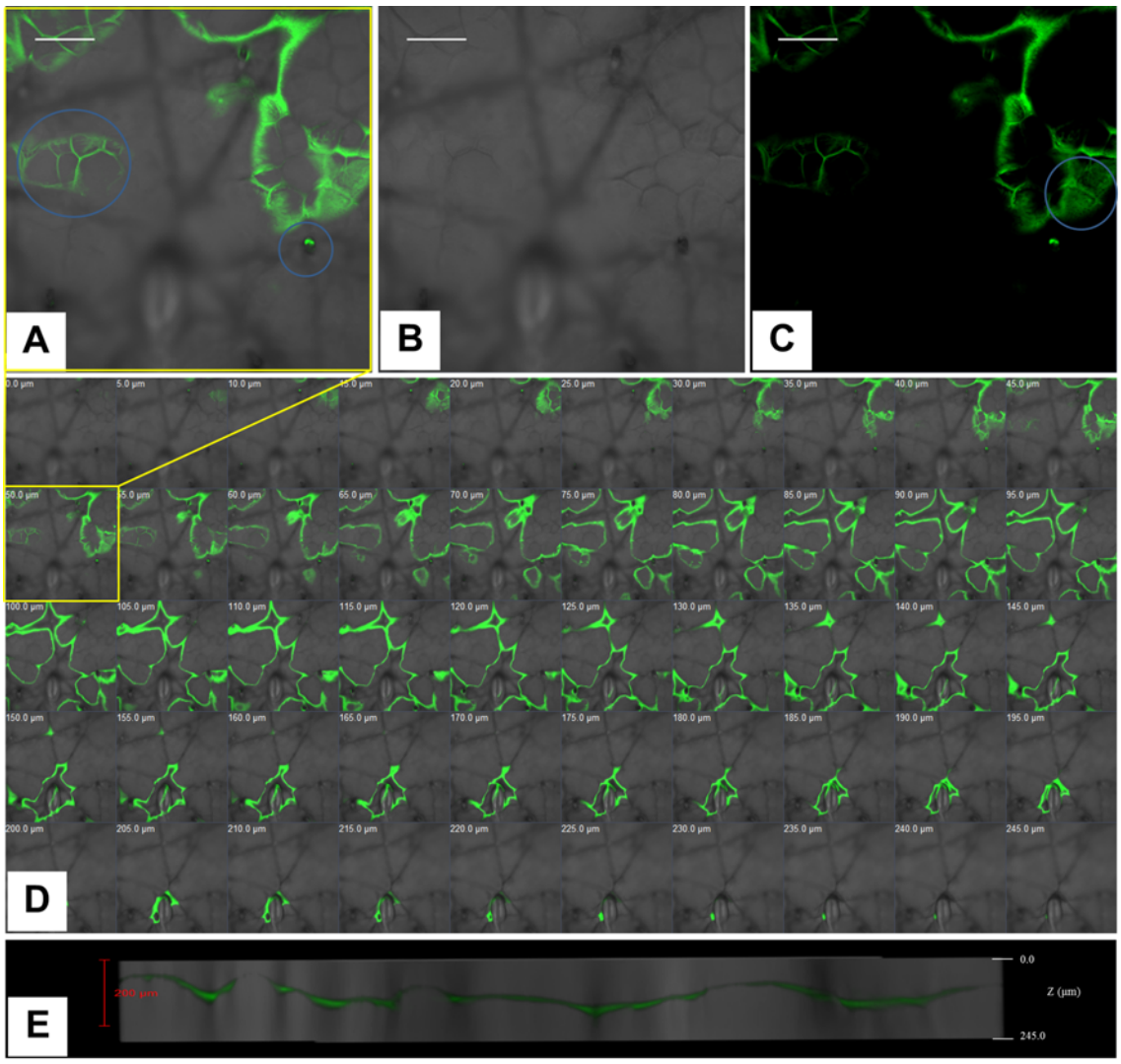

Figure 7. The optical cross-section of the skin (z=50 μm) in merge mode (A), DIC mode (B), and fluorescence mode (C) show detailed permeation pathways of FGNs through the SC. FITC-BSA (0.2% w/w) was used as a fluorescence tag to illustrate the penetration routes through the SC (t=12 h). CLSM image represents the different depths of the skin from the surface (0-245 μm at 5 μm intervals) (D). The vertical-section (z-axis) of the skin was generated through the digitized image data of the successive xy-planes (0-245 μm at 5 μm intervals) (E). (Scale bars=200 μm).

6(C) because the size of hair follicle shown in Figure 7(A) conformed to the thickness of hairs found in Figure 5 and Figure S3. Lastly, the detected green fluorescent signals in a blue circle of Figure 7(C) demonstrated that the FGN also permeated through the corneocytes membrane (*i.e*., transcellular route) showing compact and dense green fluorescent signals as illustrated in Figure 6(C). In conclusion, the green fluorescent signals of FITC-BSA within the SC structure were observed in Figure 7(A)-(C) through the matrix between the cells, the hair follicle and the corneocytes membrane. Therefore, the obtained CLSM images of Figure 7 illustrate that the FITC-BSA was delivered *via* intercellular, follicular as well as transcellular route.

Conclusions

Previously, polymeric nanoparticles have been developed mainly to deliver hydrophobic drugs to the dermis layer and its penetration mechanisms were categorized and described depending on the lipophilicity of encapsulated macromolecules due to the highly lipophilic nature of skin.[39] In our study, we have demonstrated the suitability of GNs as an approach for transdermal penetration of hydrophilic macromolecule. Fabricated GNs existed as fine individual particles without any aggregation during the storage (up to 7 days at room temperature) and enabled significant penetration enhancement (compared with control) by transporting encapsulated FGNs through the SC. In addition, GNs did not exhibit any growth inhibitory effect or presented significant cytotoxicity on cells at concentrations up to 5 mg/mL. As the skin penetration study using nanogels have rarely been explored, this study showed that gelatin-based nanogels can be optimized for transdermal delivery applications. Further study is required to demonstrate how the nature of polymeric nanoparticles affects penetration mechanism through the skin architecture. For instance, characterization of factors that alter penetration mechanisms such as increased level of SC hydration, interaction between nanoparticles and intercellular proteins and disruption of lipid packing in SC by nanoparticles should provide further improvements in designing transdermal delivery systems.[40]

Acknowledgments. This article was supported by a grant from the Korean Health Technology R&D Project, Ministry of Health and Welfare, Republic of Korea (HI13C1256 and the High Value-added Food Technology Development Program from the Korea Institute of Planning and Evaluation for Technology in Food, Agriculture, Forestry and Fisheries (iPET) (Grant number: 314058-03). The authors declare no conflicts of interest related to the content of this article.

Supporting Information: Supporting Information is available regarding the experimental procedure for the preparation of gelatin methacryloyl nano gels and skin penetration images.

References

(1) O. C. Farokhzad and R. Langer, *ACS Nano*, **3**, 16 (2009).
(2) J. Shi, A. R. Votruba, O. C. Farokhzad, and R. Langer, *Nano Lett.*, **10**, 3223 (2010).
(3) M. M. Yallapu, M. Jaggi, and S. C. Chauhan, *Drug Discov. Today*, **16**, 457 (2011).
(4) M. M. Yallapu, M. K. Reddy, and V. Labhasetwar, in *Biomedical Appl. Nanotechnol.*, John Wiley & Sons, Inc., New Jersey, 2007, p 131.
(5) P. G. Kakadia and B. R. Conway, *Am. J. Pharmacol. Sci.*, **2**, 1 (2014).
(6) S. Zhang, J. Ermann, M. D. Succi, A. Zhou, M. J. Hamilton, B. Cao, J. R. Korzenik, J. N. Glickman, P. K. Vemula, L. H. Glimcher, G. Traverso, R. Langer, and J. M. Karp, *Sci. Transl. Med.*, **7**, 300ra128 (2015).
(7) T. R. Hoare and D. S. Kohane, *J. Polym.*, **49**, 1993 (2008).
(8) A. S. Hoffman, *Adv. Drug Deliv. Rev.*, **64**, 18 (2012).
(9) B. V. Slaughter, S. S. Khurshid, O. Z. Fisher, A. Khademhosseini, and N. A. Peppas, *Adv. Mater.*, **21**, 3307 (2009).
(10) J. Groll, S. Singh, K. Albrecht, and M. Moeller, *J. Polym. Sci., Park A: Polym. Chem*., **47**, 5543 (2009).
(11) K. Ogawa, A. Nakayama, and E. Kokufuta, *Langmuir*, **19**, 3178 (2003).
(12) B. Vincent, in *Surface Chemistry in Biomedical and Environmental Science*, Springer, Dordrecht, 2006, pp 11-22.
(13) S. V. Vinogradov, T. K. Bronich, and A. V. Kabanov, *Adv. Drug Deliv. Rev.*, **54**, 135 (2002).
(14) A. Ammala, *Int. J. Cosmet. Sci.*, **35**, 113 (2013).
(15) L. S. Nair and C. T. Laurencin, *Prog. Polym. Sci.*, **32**, 762 (2007).
(16) M. R. Prausnitz and R. Langer, *Nat. Biotechnol.*, **26**, 1261 (2008).
(17) M. Kong, H. Park, C. Feng, L. Hou, X. Cheng, and X. Chen, *Carbohydr. Polym*., **94**, 634 (2013).
(18) D. A. Godwin, N.-H. Kim, and L. A. Felton, *Eur. J. Pharm. Biopharm.*, **53**, 23 (2002).
(19) M. R. Prausnitz, S. Mitragotri, and R. Langer, *Nat. Rev. Drug Discov.*, **3**, 115 (2004).
(20) K. Y. Lee and D. J. Mooney, *Prog. Polym. Sci.*, **37**, 106 (2012).
(21) J. M. Knipe, L. E. Strong, and N. A. Peppas, *Biomacromolecules*, **17**, 788 (2016).
(22) B. E. Polat, D. Blankschtein, and R. Langer, *Expert Opin. Drug Deliv.*, **7**, 1415 (2010).
(23) T. Subongkot, N. Wonglertnirant, P. Songprakhon, T. Rojanarata, P. Opanasopit, and T. Ngawhirunpat, *Int. J. Pharm.*, **441**, 151 (2013).
(24) J. W. Nichol, S. T. Koshy, H. Bae, C. M. Hwang, S. Yamanlar, and A. Khademhosseini, *Biomaterials*, **31**, 5536 (2010).
(25) K. Yue, G. Trujillo-de Santiago, M. M. Alvarez, A. Tamayol, N. Annabi, and A. Khademhosseini, *Biomaterials*, **73**, 254 (2015).
(26) A. I. Van Den Bulcke, B. Bogdanov, N. De Rooze, E. H. Schacht, M. Cornelissen, and H. Berghmans, *Biomacromolecules*, **1**, 31 (2000).
(27) P. C. Hiemenz, *Principles of Colloid and Surface Chemistry*, Marcel Dekker, New York, 1986.
(28) S. Bingaman, V. H. Huxley, and R. E. Rumbaut, *Microcircu-*

lation, **10**, 221 (2003).
(29) F. D. Malkinson, *J. Invest. Dermatol.*, **31**, 19 (1958).
(30) S. Monash, *J. Invest. Dermatol.*, **29**, 367 (1957).
(31) M. Förster, M.-A. Bolzinger, H. Fessi, and S. Briançon, *Eur J Dermatol*., **19**, 309 (2009).
(32) A. Lauterbach and C. C. Muller-Goymann, *Eur. J. Pharm. Biopharm.*, **97**, 152 (2015).
(33) J. J. Escobar-Chávez, *Skin*, **19**, 22 (2012).
(34) P. Volz, A. Boreham, A. Wolf, T.-Y. Kim, J. Balke, J. Frombach, S. Hadam, Z. Afraz, F. Rancan, U. Blume-Peytavi, A. Vogt, and U. Alexiev, *Int. J. Mol. Sci.*, **16**, 6960 (2015).
(35) G. Cevc and U. Vierl, *J. Control. Release*, **141**, 277 (2010).
(36) H. Cui, P. Quan, H. Zhao, X. Wen, W. Song, Y. Xiao, Y. Zhao, and L. Fang, *J. Pharm. Sci.*, **104**, 3395 (2015).
(37) P. Garidel, *Phys. Chem. Chem. Phys.*, **4**, 5671 (2002).
(38) J. Hadgraft and M. E. Lane, *Phys. Chem. Chem. Phys.*, **13**, 5215 (2011).
(39) A. Alkilani, M. T. McCrudden, and R. Donnelly, *Pharmaceutics*, **7**, 438 (2015).
(40) L. S. Nair and C. T. Laurencin, *Prog. Polym. Sci.*, **32**, 762 (2007).